

Electron detachment and fragmentation of laser-excited rotationally hot Al_4^- B. Kafle,¹ O. Aviv,¹ V. Chandrasekaran,¹ O. Heber,¹ M. L. Rappaport,¹ H. Rubinstein,¹ D. Schwalm,^{1,2,*}
D. Strasser,³ and D. Zajfman¹¹*Department of Particle Physics, Weizmann Institute of Science, Rehovot 76100, Israel*²*Max-Planck-Institut für Kernphysik, D-69117 Heidelberg, Germany*³*Institute of Chemistry, Hebrew University of Jerusalem, Jerusalem 91904, Israel*

(Received 23 July 2015; published 2 November 2015)

Absolute photoabsorption cross sections of negatively charged tetra-atomic aluminum clusters have been measured for photon energies between 1.8 and 2.7 eV. The experiment used the depletion technique in combination with an electrostatic ion-beam trap, in which Al_4^- ions produced in a sputter ion source were stored for 90 ms before being subjected to a short laser pulse. Moreover, the competition between one-atom fragmentation and electron emission of the laser-excited Al_4^- has been measured. These measurements show that fragmentation dominates electron emission at all photon energies below the electron attachment energy of ~ 2.2 eV, even though the fragmentation energy is expected to be 10%–20% higher than the electron attachment energy. These findings, when taken together with the delayed-electron and fragmentation yields observed in a previous measurement [O. Aviv *et al.*, *Phys. Rev. A* **83**, 023201 (2011)], can be well explained within the statistical phase-space theory for unimolecular decays assuming the Al_4^- ions to be rotationally hot. The analysis permits the determination of the adiabatic electron detachment energy of Al_4^- to be $E_{\text{ad}} = (2.18 \pm 0.02)$ eV and the one-atom fragmentation energy to be $D_0 = (2.34 \pm 0.05)$ eV. Moreover, two direct *s*-wave ionization channels are observed with threshold energies of (2.18 ± 0.02) eV and (2.45 ± 0.02) eV.

DOI: [10.1103/PhysRevA.92.052503](https://doi.org/10.1103/PhysRevA.92.052503)

PACS number(s): 36.40.Qv, 33.80.Eh, 36.40.Vz, 37.10.Ty

I. INTRODUCTION

One of the intriguing properties of hot isolated clusters, even those containing only a few atoms, is the occurrence of delayed electron and atom emission, which are mediated via processes that can be considered to be the microscopic analogs of the thermionic emission of electrons and atoms from surfaces of the bulk material [1]. In fact, the delayed emission of electrons, atoms, and photons has been established as an important decay channel for excited clusters and statistical approaches and thermodynamical concepts have been developed and employed to describe theoretically the underlying processes [2,3].

Charged cluster ions are particularly well suited to studying these processes in detail: Their charge allows for easy mass selection and long-term storage of the ions by electromagnetic fields and after being excited their decay into the various channels can be readily analyzed as a function of time. Employing an electrostatic ion-beam trap (EIBT) to store and precool the cluster ions and using short laser pulses to excite them by a well-defined amount of energy, we have recently investigated in a series of experiments the prompt and delayed emission processes occurring in small negative aluminum clusters [4–8]. Although Al_n^- cluster anions have already been under experimental [9–21] and theoretical [22–31] scrutiny for many years, the experimental focus was mainly on the electronic properties of these clusters as they are considered to be a prototype for metal clusters formed out of multivalent atoms. Only limited experimental information has been available about the decay dynamics of hot small Al_n^- ions and the corresponding energetic thresholds, which is indispensable when aiming at a detailed understanding of the decay processes and their competition.

Our interest in anionic aluminum clusters was actually triggered by the prospect of studying the radiative cooling of hot clusters using delayed electron emission as a thermometer to determine the temperature of the ions [4]. The smallest Al_n^- cluster found to exhibit delayed electron emission on time scales covered by our setup ($\gtrsim 10 \mu\text{s}$) was the tetramer Al_4^- and despite containing only four atoms, the detachment process and the radiative cooling were found to be reasonably well described within a thermodynamical framework.

To get more microscopic insight into the delayed decay processes occurring in Al_4^- , we systematically studied in a follow-up experiment the competition between electron detachment ($\text{Al}_4^- + h\nu \rightarrow \text{Al}_4^{-*} \rightarrow \text{Al}_4 + e^-$) and one-atom fragmentation ($\text{Al}_4^- + h\nu \rightarrow \text{Al}_4^{-*} \rightarrow \text{Al}_3^- + \text{Al}$) at various storage times for photon energies $E_\lambda = h\nu$ between ~ 1.5 and ~ 2.6 eV [5,7]. Although the dissociation energy D_0 connected with the one-atom fragmentation was predicted [24] to be well above the adiabatic electron detachment energy E_{ad} of about 2.2 eV, we observed at all photon energies below ~ 2.2 eV delayed atom and delayed electron emission, the delayed atom emission even dominating the delayed electron decay for $E_\lambda < 1.7$ eV. It was therefore conjectured that the one-atom dissociation energy D_0 has to be much closer to or even below the adiabatic electron detachment energy and/or that for a certain percentage of the Al_4^- ions the amount of excitation energy at their disposal to overcome the dissociation threshold is larger than the energy available for electron detachment. As atomic clusters produced in sputter ion sources are known to be vibrationally *and* rotationally hot [32], it was suggested [7] that the extra amount of energy might be supplied by the rotational energy, which can be converted into translational energy in the fragmentation process while not being retrievable in the electron detachment process.

An experimental value for the adiabatic electron detachment energy of Al_4^- of $E_{\text{ad}} = 2.20 \pm 0.05$ eV is usually

*Corresponding author: Dirk.Schwalm@mpi-hd.mpg.de

quoted in the theoretical literature [24,26,28–31], which seems to be estimated from high-resolution photoelectron spectra of Li *et al.* [14], although no details of how this value was deduced from the data are available. On the other hand, we are unaware of an experimental value for the one-atom dissociation energy D_0 of Al_4^- . It was first calculated by Rao and Jena [24] to be ~ 0.5 eV larger than E_{ad} . In the meantime, the binding energies of small charged and neutral Al_n clusters were recalculated using improved *ab initio* quantum chemical calculations [26,31]. Their most reliable calculations for Al_4^- , based on coupled-cluster theory with perturbative triple correction, result in $E_{\text{ad}} = 2.20 \pm 0.04$ eV and $D_0 = 2.38 \pm 0.06$ eV, where the uncertainties reflect the spread of their results when using different electronic basis sets. The fragmentation energies for other fragmentation channels are calculated to be at least 1 eV above D_0 .

The predicted one-atom dissociation energy being only 0.18 eV higher than the adiabatic electron detachment energy makes the conjecture of Ref. [7], that the rotational energy of the stored Al_4^- ions is responsible for the observed preponderance of the delayed fragmentation at low photon energies, even more likely. The present work is therefore intended to clarify the situation. It includes a measurement of the photoabsorption cross section of Al_4^- and of the total (prompt and delayed) branching ratio between fragmentation and electron detachment for photon energies between ~ 1.8 and ~ 2.5 eV. The measurements allows us to put the relative delayed cross sections for fragmentation and detachment determined in Ref. [7] on an absolute scale and to model their photon energy dependences. Applying unimolecular decay theory based on statistical phase-space considerations to our data set, we are able to obtain a consistent description of the competition between detachment and fragmentation. The analysis implies that the Al_4^- ions carry on average a rotational angular momentum of $\langle J \rangle \sim 125\hbar$, corresponding to a rotational temperature of ~ 1400 K, and results in a adiabatic detachment energy of $E_{\text{ad}} = (2.18 \pm 0.02)$ eV and a one-atom dissociation energy of $D_0 = (2.34 \pm 0.05)$ eV.

II. EXPERIMENTAL SETUP

The experimental arrangement used in the present work is shown schematically in Fig. 1 and has been discussed together with its properties in a previous publication [8]. In brief,

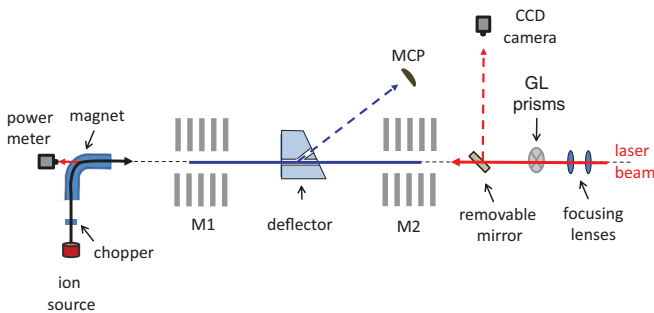


FIG. 1. (Color online) Schematic view of the experimental setup used to determine absolute photoinduced cross sections for Al_4^- anions.

Al_4^- clusters are produced in a cesium sputter ion source and accelerated to an energy of 4.2 keV. The ions are then bunched, mass selected by a 90° magnet, and injected into an EIBT, which is equipped with a central electrostatic deflector. As long as the deflector plates remain grounded, the Al_4^- clusters oscillate undisturbed between the two electrostatic mirrors M1 and M2 through a 3-mm-diam hole in the deflector. The oscillation period of the ions is $T_{\text{osc}} = 16.0 \mu\text{s}$ and as the trap is operated in the nonbunching mode [33], the ions fill the longitudinal phase space of the trap after a few milliseconds of storage. The lifetime of the stored beam is limited to typically 1 s by residual gas scattering.

After 90 ms of storage, the ions are overlapped coaxially with a short (~ 9 -ns) laser pulse, whose wavelength is tunable between 210 and 2600 nm. The laser pulse energy U , which can be varied by a Glan-Taylor polarizing prism, is measured for each pulse by a calibrated power meter located upstream of the EIBT (see Fig. 1). The laser beam waist and profile is adjusted and regularly monitored by inserting a mirror into the optical path and observing the profile of the reflected light by a CCD camera installed at a distance equal to the distance from the mirror to the deflector, whose aperture is the limiting restriction in the laser beam path. The laser beam was found to be on average reasonably well described by a symmetric Gaussian profile with a variance of 0.75 ± 0.15 mm.

By applying a voltage step to one of the two electrodes of the electrostatic deflector, clusters or charged fragments located between the deflector and M1 can be extracted mass selectively from the trap and counted by a microchannel plate (MCP) detector. This property of the setup is used to monitor the number of parent clusters (Al_4^-) present before and after the laser pulse and the number of charged fragments (Al_3^-) produced. Since these measurements are destructive, the counting of clusters and fragments has to be done alternately for consecutive injections and by averaging over a sufficient number of injections to smooth out beam fluctuations and to ensure an adequate statistical accuracy. Since the extracted ions reach the MCP detector in short bunches (spill times T_{spill} are $7.1 \mu\text{s}$ for Al_4^- and $2.3 \mu\text{s}$ for Al_3^- fragments [8]), the number of injected clusters is adjusted such that the number of ions per spill is limited to $\lesssim 30$, thereby keeping dead-time corrections to $\lesssim 10\%$. For further details concerning the measurement procedures, as well as the different collection and detection efficiencies for parent clusters and charged fragments, the reader is referred to Ref. [8].

III. MEASUREMENTS

A. Photoabsorption cross section of Al_4^-

The depletion method was used to determine the total (prompt and delayed) photoinduced destruction cross section of Al_4^- by monitoring the number of clusters stored in the trap 1 ms before and 1–2 ms after the laser pulse as a function of the laser pulse energy U . Denoting the number of detected clusters before the pulse by N_b and after the pulse by $N_a(U)$, the survival probability $P(U)$, and thus the depletion probability $D(U)$, can be directly determined from the number of extracted clusters by

$$D(U) = 1 - P(U) = 1 - N_a(U)/N_b, \quad (1)$$

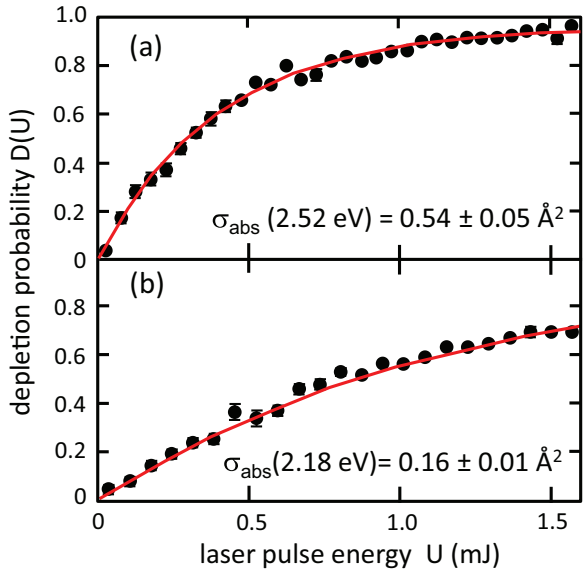


FIG. 2. (Color online) Representative depletion curves $D(U)$ for Al_4^- clusters after irradiation with photons of (a) 2.52 eV and (b) 2.18 eV contained in a 9-ns-long laser pulse with pulse energies U up to 1.5 mJ (circles with statistical error bars). The clusters were stored for 90 ms before the laser pulse. The solid (red) curves are the result of fits to the experimental data, the photoabsorption cross section $\sigma_{\text{abs}}(E_\lambda)$ being the only free parameter.

since the ratio between stored and detected clusters is the same in both measurements. Moreover, as the time between the two measurements is short compared to the lifetime of the cluster in the trap, additional losses between the two measurements due to residual gas scattering can be neglected. On the other hand, the waiting time after the laser pulse is sufficiently long to allow also for delayed decays, which are known to occur within a few hundred microseconds [7], to take place before the measurement. Examples of depletion curves for Al_4^- clusters, induced after a storage time of 90 ms by a laser pulse with photons of 491 nm (2.52 eV) and 568 nm (2.18 eV) and pulse energies up to 1.5 mJ, are presented in Figs. 2(a) and 2(b), respectively. At these wavelengths, the absorption of one photon is sufficient to lift all Al_4^- ions, regardless of their internal excitation energy at the time of the laser shot, above the lowest destruction threshold given by the adiabatic electron detachment energy. In these cases, the probability of the excited ions to decay by either electron emission or fragmentation is expected to be one as stabilization decays by photon emission are much slower and can be neglected. The destruction cross section is thus equal to the photon absorption cross sections $\sigma_{\text{abs}}(E_\lambda)$ and the latter can be directly deduced from the depletion curves using the procedure discussed in Ref. [8]. The solid curves shown in Figs. 2(a) and 2(b) are the result from χ^2 fits of the measured depletion curves with $\sigma_{\text{abs}}(E_\lambda)$ being the only free parameter. The resulting cross sections $\sigma_{\text{abs}}(E_\lambda)$ are given with their statistical uncertainties.

At photon energies $E_\lambda < E_{\text{ad}}$, the destruction of an ion with vibrational energy E_v and rotational energy E_r fulfilling $E_v + E_\lambda \lesssim \min\{E_{\text{ad}}, D_0 - E_r\}$ cannot be induced by a one-photon process but requires the absorption of a second photon from the

laser pulse. Since the relaxation of the optically excited Al_4^- state after the absorption of the first photon into vibrational motion is fast compared to the length of the photon pulse [34], the second photon will be absorbed by a vibrationally highly excited Al_4^- with an absorption cross section $\sigma_{\text{abs},2}(E_\lambda)$. Under these circumstances the depletion probability $D(U)$ is given by Eq. (11) of Ref. [8] with, using the nomenclature of [8], $p(z,r;U)$ being replaced by

$$p(z,r;U) = p_1(z,r;U) + [1 - G(E_\lambda)] \frac{\sigma_{\text{abs}}}{\sigma_{\text{abs}} - \sigma_{\text{abs},2}} \times [p_2(z,r;U) - p_1(z,r;U)]. \quad (2)$$

Here $p_i(z,r;U)$ are given by Eq. (10) of [8] with $\sigma = \sigma_{\text{abs}}$ for $i = 1$ and $\sigma = \sigma_{\text{abs},2}$ for $i = 2$ and $G(E_\lambda)$ denotes the percentage of the ions for which the absorption of one photon is sufficient to lead to destruction.

The statistical accuracy of our data does not allow the determination of the two absorption cross sections and $G(E_\lambda)$ from the measured depletion curve. In a first analysis step, we therefore estimate the probability $G(E_\lambda)$ by using a Boltzmann distribution for 600 K to describe the internal vibrational energy distribution of the Al_4^- ions after 90 ms of storage [4] and assume $D_0 - \langle E_r \rangle = E_{\text{ad}} = 2.2$ eV. The resulting probabilities decrease smoothly from $G = 1$ via 0.6 to 0.13 for $E_\lambda = 2.2, 2.0$, and 1.8 eV, respectively. In a second step we then use the final result of our statistical model analysis (Sec. V) to calculate $G(E_\lambda)$ and repeat the fits of the depletion curves. The model values for $G(E_\lambda)$ are found to be close to the values used in the first analysis step and the resulting changes of the absorption cross sections are well within their statistical errors. Setting $\sigma_{\text{abs},2}(E_\lambda) = \beta \sigma_{\text{abs}}(E_\lambda)$, the fits of the depletion curves observed for $E_\lambda < 2.18$ eV result in β values scattering by about 25% around $\beta = 0.35$. The final χ^2 fits are therefore performed by setting $\beta = 0.35 \pm 0.10$. Two examples are displayed in Fig. 3; the errors given for the extracted absorption cross sections $\sigma_{\text{abs}}(E_\lambda)$ include the statistical errors as well as the uncertainties caused by $G(E_\lambda)$ and β .

Figure 4 displays the absorption cross sections $\sigma_{\text{abs}}(E_\lambda)$ for Al_4^- clusters stored and cooled for 90 ms as a function of the photon energy E_λ . While the errors shown (typically $\pm 15\%$) are dominated by statistical errors, the absolute scale is subject to an additional systematic error of $\pm 20\%$ mainly caused by the measurement of the laser pulse energy [5]. For photon energies below 2.18 eV, where the photon absorption results in a vibrationally highly excited Al_4^{-*} , the absorption cross section is found to decrease with increasing photon energies. At photon energies above 2.18 eV the absorption cross section increases in two steps up to $\sim 0.7 \text{ \AA}^2$ at $E_\lambda \sim 2.6$ eV. We attribute this stepwise increase to the opening of two direct ionization channels leading to $\text{Al}_4 + e^-$.

To parametrize $\sigma_{\text{abs}}(E_\lambda)$, we approximate the absorption cross section $\sigma_{\text{abs}}^*(E_\lambda)$ leading to Al_4^{-*} by an exponential, i.e., $\sigma_{\text{abs}}^*(E_\lambda) = \sigma_0^* \exp(-aE_\lambda)$, with $\sigma_0^* = 9.6 \text{ \AA}^2$ and $a = 2.1 \text{ eV}^{-1}$. The direct ionization channels are described by a generic cross section of the form [35]

$$\sigma_i(E_\lambda) = \sigma_{0,i}(E_\lambda - E_{0,i})^{l_i+1/2}/E_\lambda^3, \quad (3)$$

with $E_{0,i}$ being the ionization threshold and $l_i = 0$ (1) for s (p) electrons, which reduces to the corresponding Wigner threshold laws for $E_\lambda \rightarrow E_{0,i}$. While we cannot exclude contributions of direct p -wave channels to $\sigma_{\text{abs}}(E_\lambda)$, a reasonable description of $\sigma_{\text{abs}}(E_\lambda)$ over the range of measured photon energies can be obtained, as shown by the solid curve in Fig. 4, which was calculated setting $\sigma_{\text{abs}}(E_\lambda) = \sigma_{\text{abs}}^*(E_\lambda) + \sigma_1(E_\lambda) + \sigma_2(E_\lambda)$ with $E_{0,1} = 2.18$ eV, $E_{0,2} = 2.45$ eV, $l_1 = l_2 = 0$, and adjusting $\sigma_{0,i}$. Note that the extrapolation of $\sigma_{\text{abs}}^*(E_\lambda)$ to energies $E_\lambda > 2.18$ eV (dashed curve in Fig. 4) is not mandatory to ensure a reasonable description of $\sigma_{\text{abs}}(E_\lambda)$. However, as shown in Fig. 7 and discussed in Sec. V, the extrapolated cross section leads to fragmentation branching ratios consistent with the experimental values.

The onsets of the two direct s -wave ionization channels appear to be well defined within ± 0.02 eV. This is not *a priori* expected due to the vibrational excitation of the Al_4^- anions and the verticality of the photon absorption process, which can lead to a distribution of threshold energies whose width depends on the geometry differences between the initial and final electronic states in Al_4^- and Al_4 , respectively. Although the data certainly allow for some broadening of the threshold energies, the reasonable description of the onset behavior by Eq. (3) suggests that these geometry differences are small and that the deduced threshold energies are thus approximately reflecting the (adiabatic) excitation energies of the final electronic states of Al_4 with respect to the electronic ground state of Al_4^- .

B. Fragmentation of photoexcited Al_4^-

The only fragmentation channel open for photoexcited Al_4^{-*} at photon energies investigated in this work is the monomer channel leading to $\text{Al}_3^- + \text{Al}$. As the fragmentation can involve delay times up to 200 μs [7], we first investigated

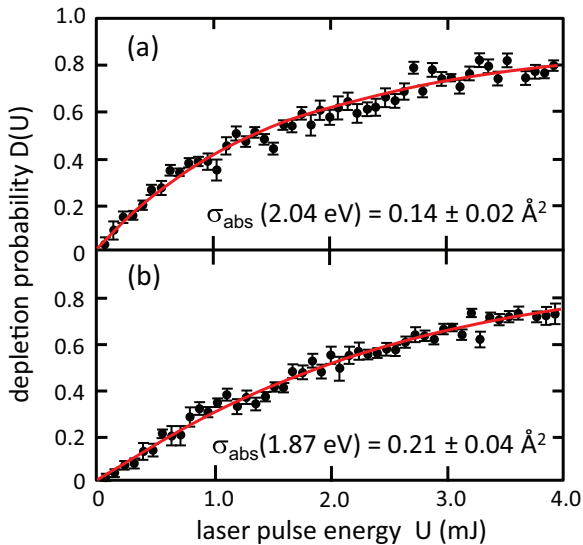


FIG. 3. (Color online) Same as Fig. 2, but for photon energies of (a) 2.04 eV and (b) 1.87 eV and pulse energies U up to 4 mJ (circles with statistical error bars). The quoted absorption cross sections $\sigma_{\text{abs}}(E_\lambda)$ result from least-squares fits of the depletion curves, as discussed in the text [solid (red) curves].

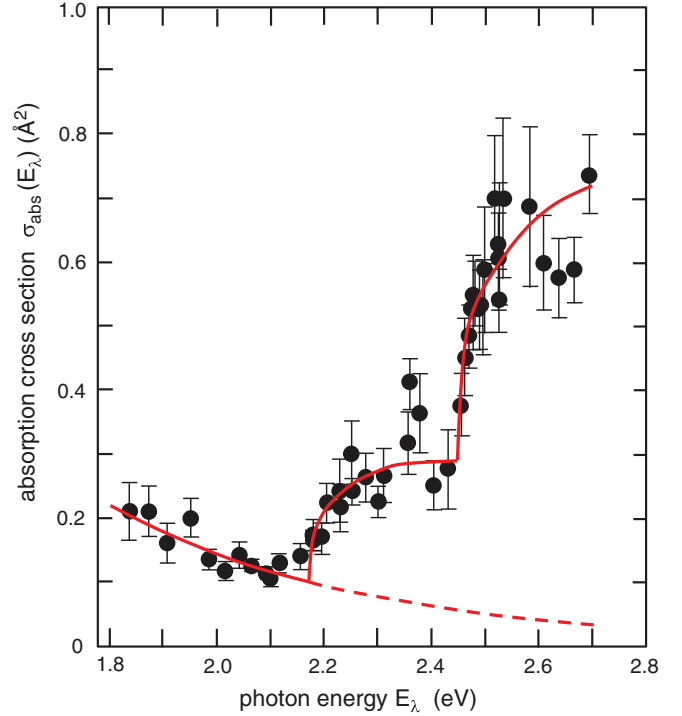


FIG. 4. (Color online) Measured photoabsorption cross sections $\sigma_{\text{abs}}(E_\lambda)$ of Al_4^- clusters as a function of the photon energy E_λ (circles with error bars). The data were taken 90 ms after injecting the Al_4^- clusters into the trap. The solid (red) curves represent a parametrization of $\sigma_{\text{abs}}(E_\lambda)$ as discussed in the text, assuming the absorption cross section $\sigma_{\text{abs}}^*(E_\lambda)$ for energies greater than 2.2 eV to be given by the dashed (red) line.

for a few characteristic photon energies the relative contribution of the delayed events to the total fragmentation yield, information that is required to determine the total (prompt and delayed) fragmentation probabilities $b_f(E_\lambda)$ and to put the relative delayed fragmentation and electron detachment yields measured in Ref. [7] on an absolute scale.

The delay-time dependence of the Al_3^- fragments is measured by counting, alternately for consecutive injections, the number of Al_4^- clusters N_b extracted from the trap at $\hat{t} = -1$ ms and the number of Al_3^- fragments $N_f(U, \hat{t})$ extracted at $\hat{t} = t_{\text{def}} - t_{\text{las}}$, where t_{def} denotes the time at which the voltage step is applied to the deflector while t_{las} denotes the time at which the laser pulse is fired. The relative fragmentation probability $N_f(U, \hat{t})/N_b$, measured as a function of \hat{t} while keeping the laser pulse energy constant at $U \approx 0.3$ mJ, is displayed in Fig. 5 for three photon energies.

The fragmentation probability measured at a photon energy of 2.48 eV mainly reflects the well-understood time dependence expected for prompt fragmentation, that is, for fragmentations occurring in times much shorter than the time resolution of our setup ($T_{\text{spill}} = 2.3$ μs); the few events seen at later times are likely due to prompt fragments that, by chance, manage to stay in the trap for one round-trip. For photon energies below 2.2 eV, however, delayed fragmentation events are clearly observed. As shown in Ref. [7], the time dependence $f(t)$ of the delayed fragmentation yield can be reasonably well described by a power law $f(t) \propto t^{-\alpha_f}$ in the relevant time

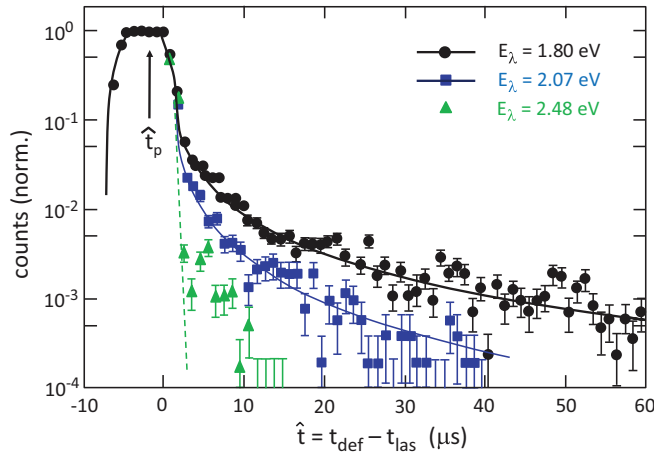


FIG. 5. (Color online) Relative fragmentation probability $N_f(U, \hat{t})/N_b$ of Al_3^- fragments as function of the time difference \hat{t} between the switching time of the deflector voltage and the time of the laser pulse. The Al_4^- parent clusters were stored for 90 ms before being exposed to a laser pulse with an average pulse energy U of 0.3 mJ. The distributions were normalized to one at $\hat{t} = \hat{t}_p = -2.0 \mu\text{s}$. The dashed (green) line reflects the fragmentation probability in the case in which all fragmentations occur promptly, i.e., within submicrosecond times. The solid lines are fits of the data using a model function to describe the delay time dependence of the fragmentation process (see the text).

regime. By limiting the power law to decay times $t \geq t_0$ and using a δ function to account for decay times $t < t_0$ (with $t_0 < T_{\text{spill}}$), the solid lines shown in Fig. 5 are obtained after folding $f(t)$ with the collection efficiency of our setup and adjusting α_f . The fits result in $\alpha_f = 1.64 \pm 0.16$, 1.75 ± 0.17 , and 1.95 ± 0.19 for the measurements at photon energies of 1.80, 2.00, and 2.07 eV, respectively, in good agreement with the findings of Ref. [7].

The measurements show that at all investigated photon energies the contribution of the delayed fragmentation to the total fragmentation yield is small and that the prompt Al_3^- yield measured at $\hat{t} = \hat{t}_p = -2 \mu\text{s}$ closely represents the total fragmentation yield. The total branching ratio $b_f(E_\lambda)$ can thus be determined as discussed in Ref. [8] by comparing $N_f(U, \hat{t}_p)/N_b$ to the depletion probability $D(U)$ of Al_4^- . This is done by counting, again, alternately for consecutive injections, the number of Al_4^- clusters extracted from the trap at $\hat{t} = -1 \text{ ms}$ (N_b) and $\hat{t} = 1 \text{ ms}$ [$N_a(U)$], as well as the number of Al_3^- fragments $N_f(U, \hat{t}_p)$ extracted at \hat{t}_p . In contrast to the depletion probability $D(U)$, which can be directly determined from $N_a(U)$ and N_b [Eq. (1)], for extracting the absolute fragmentation probability, the ratio ζ of the collection and detection efficiencies for the parent clusters Al_4^- to that of the Al_3^- fragments has to be taken into account. The total absolute fragmentation probability $P_f(U)$ is thus given by

$$P_f(U) = \frac{N_f(U, \hat{t}_p)}{N_b} \zeta [1 + \eta_f(E_\lambda)], \quad (4)$$

with $\zeta = 3.1 \pm 0.3$ [8]. The function $\eta(E_\lambda)$, which corrects for the percentage of delayed fragmentations outside the prompt window, was calculated from the time dependence of the fragmentation yield $f(t)$ fitted to the $N_f(U, \hat{t})/N_b$ curves

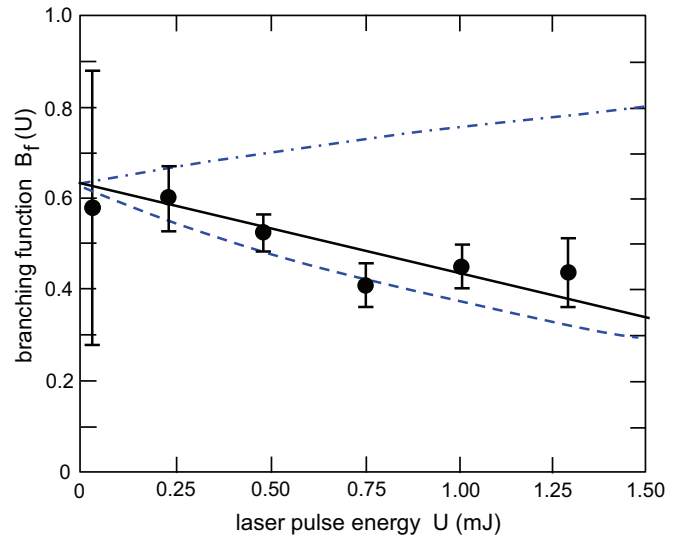


FIG. 6. (Color online) Branching function $B_f(U)$ measured for the monomer fragmentation channel as a function of laser pulse energy U , subjecting Al_4^- after 90 ms of storage to a short laser pulse of 1.91-eV photons. The solid line represents a linear fit to the data. The dashed and dash-dotted (blue) lines are calculated branching functions that include two-photon excitation processes for two extreme scenarios (see the text for more details).

measured at $E_\lambda = 1.80, 2.00, \text{ and } 2.07 \text{ eV}$ and interpolated for other photon energies; $\eta_f(E_\lambda)$ was found to be less than 0.15 for all relevant photon energies.

Following [8], we define a branching function $B_f(U)$ by

$$B_f(U) = \frac{P_f(U)}{D(U)}, \quad (5)$$

from which we can determine b_f by extrapolating $B_f(U)$ towards the vanishing pulse energy limit $U = 0$, i.e.,

$$b_f = \lim_{U \rightarrow 0} B_f(U) \frac{F_0}{F_f}, \quad (6)$$

where F_0 and F_f describe the overlap of the laser beam and the stored ion beam for the depletion and appearance process, respectively [8]. In the present experiment, $F_0/F_f = 1.07$. For clarity, we would like to point out that the total branching ratio b_f is defined here as the ratio of the fragmentation probability to the sum of the probability for fragmentation and detachment and that total is added to explicitly indicate that prompt and delayed contributions are included in the ratio.

To illustrate the extrapolation procedure, the branching function $B_f(U)$ observed when irradiating Al_4^- with a pulse of 1.91-eV photons is displayed in Fig. 6 together with a least-squares fit of a straight line to the data. This results in $B_f(0) = 0.62 \pm 0.10$, which leads to $b_f = 0.67 \pm 0.10$. The dependence of $B_f(U)$ on U is determined by the two-photon contributions to the fragmentation, i.e., by $\sigma_{\text{abs},2}(E_\lambda)$ and the branching ratio $b_{f,2}$ of the highly excited Al_4^{*-} state. Fixing $B_f(0)$ at 0.62, the two broken curves plotted in Fig. 6 reflect two extreme scenarios, namely, $b_{f,2} = 0$ (dashed line) and $b_{f,2} = 1$ (dash-dotted line). The solid line corresponds to $b_{f,2} \approx 0.2$, which is consistent with the decay rate coefficients estimated in Sec. V for vibrational energies of $\approx 3.8 \text{ eV}$.

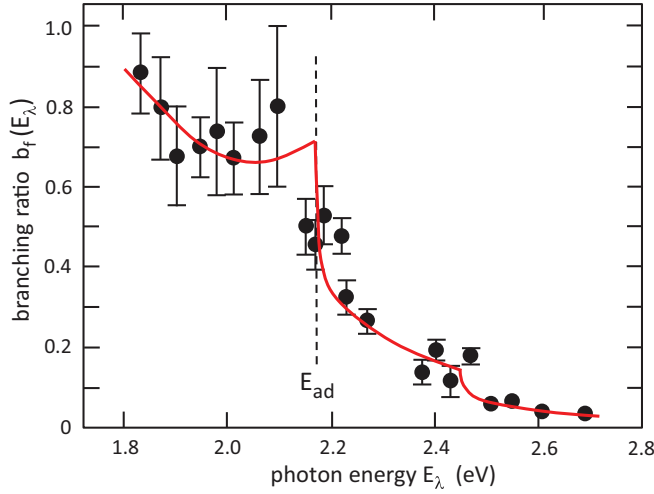


FIG. 7. (Color online) One-photon-induced total branching ratio $b_f(E_\lambda)$ measured in the present study for the fragmentation of laser-excited Al_4^- clusters into $\text{Al}_3^- + \text{Al}$ as a function of photon energy (circles with error bars). The Al_4^- clusters were stored for 90 ms before being subjected to the laser pulse. The vertical dashed line denotes the position of the adiabatic detachment energy E_{ad} . The solid (red) curve is the result of our statistical model calculation discussed in Sec. V.

It should be noted, however, that by extrapolating $B_f(U)$ to $U = 0$ it is ensured that only one-photon processes are contributing to the branching ratio $b_f(E_\lambda)$.

The total branching ratios for one-atom emission from laser-excited Al_4^- clusters, which were allowed to cool for 90 ms before their excitation, were measured for photon energies between 1.8 and 2.7 eV. The results are displayed in Fig. 7. Notably, these total ratios show the same behavior already observed when studying the delayed branching ratios [7], namely, an increase for decreasing photon energies and even domination of the electron emission for photon energies smaller than the adiabatic detachment energy, opposite to what one would naively expect for the decay of a cluster where the dissociation energy D_0 is larger than the electron detachment energy E_{ad} .

C. Absolute delayed cross sections for fragmentation and electron detachment

In an earlier experiment [7], we determined the relative cross sections for delayed electron detachment and delayed one-atom fragmentation of laser-excited Al_4^- for photon energies between 1.4 and 2.4 eV. In these measurements, the laser pulse energies U were kept below 0.08 mJ to ensure that only one-photon excitations were taking place. The delayed cross section, measured at four storage times between 100 and 400 ms, were obtained up to a common constant factor by summing the corresponding yields observed for delay times in the range $12 \mu\text{s} \leq t \leq 188 \mu\text{s}$ with respect to the time the laser was fired.

To put these relative cross sections on an absolute scale, we use the relative fragmentation probabilities measured in Sec. III B at three photon energies of 1.80, 2.00, and 2.07 eV to calculate the ratio $R_d(E_\lambda)$ of delayed to total fragmentation by

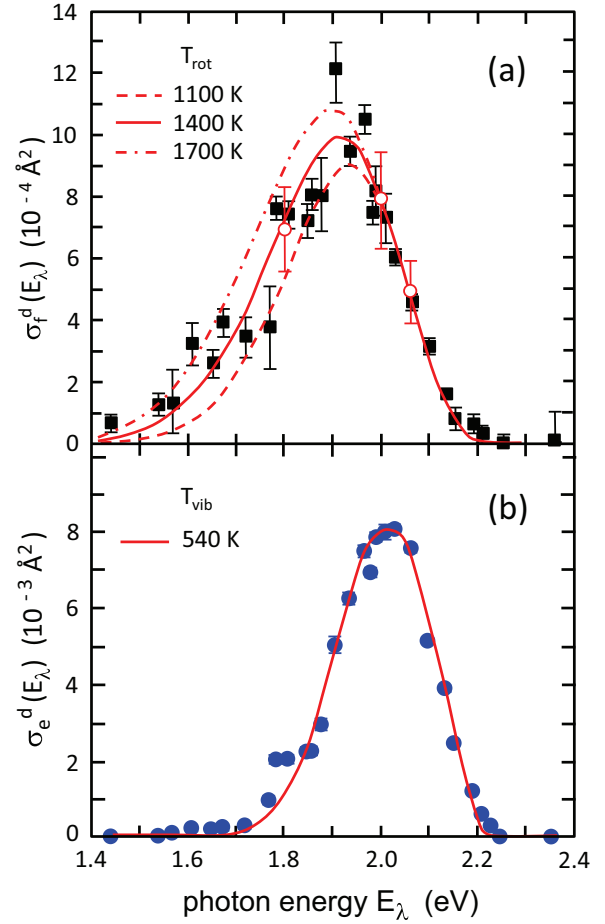


FIG. 8. (Color online) (a) Delayed fragmentation and (b) delayed electron detachment cross section for Al_4^- ions stored for 100 ms before laser excitation. The relative data (circles with error bars) are taken from Ref. [7] and scaled to fit the absolute values determined in the present work at three photon energies [open red circles in (a)]. The red lines are the result of our statistical model calculation discussed in Sec. V.

integrating the fitted $f(t)$ functions over the respective decay times t . This results in $R_d(E_\lambda) = 0.023 \pm 0.003$, 0.012 ± 0.002 , and 0.0054 ± 0.0010 for $E_\lambda = 1.80, 2.00$, and 2.07 eV, respectively. Together with the measured absorption cross section $\sigma_{\text{abs}}^*(E_\lambda)$, the fraction $G(E_\lambda)$ of Al_4^- that can be destroyed by one-photon absorption, and the branching ratio $b_f(E_\lambda)$ determined in the preceding section, we can calculate the absolute delayed fragmentation cross section $\sigma_f^d(E_\lambda)$ at these photon energies by

$$\sigma_f^d(E_\lambda) = \sigma_{\text{abs}}^*(E_\lambda)G(E_\lambda)b_f(E_\lambda)R_d(E_\lambda). \quad (7)$$

The resulting values are displayed in Fig. 8(a) by the open circles together with the delayed fragmentation cross sections obtained by Aviv *et al.* after 100 ms of storage [Fig. 10(b) of Ref. [7]], which were scaled to the three absolute values, neglecting the 10-ms difference in storage times between the two measurements. The same scaling factor was then applied to the corresponding measurement of the delayed electron detachment cross sections [Fig. 10(a) of Ref. [7]]; the result is shown in Fig. 8(b). The errors given are the statistical errors

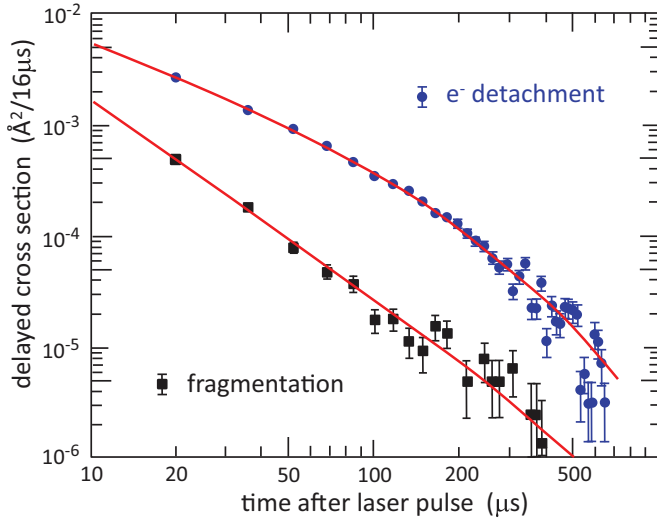


FIG. 9. (Color online) Time dependence of the electron detachment and fragmentation cross section of Al_4^- , which was stored for 100 ms before being excited by photons of 1.965 eV. The data (circles with error bars) are taken from Ref. [7] and scaled as discussed in the text. The solid (red) lines are the result of our statistical model calculation discussed in Sec. V.

of the original measurement. Note, however, that the scale of $\sigma_e^d(E_\lambda)$ is subject to a systematic uncertainty of 30% as the cross section for delayed electron emission relative to the delayed fragmentation could only be determined in [7] to within this accuracy.

The scaling factor was also used to normalize the time-dependent detachment and fragmentation signal observed after the absorption of 1.965-eV photons by Aviv *et al.* (Fig. 4 of Ref. [7]). The normalized data are displayed in Fig. 9.

IV. STATISTICAL MODEL CALCULATIONS

Clusters extracted from sputter ion sources are known to be produced with high vibrational T_{vib} and rotational temperatures T_{rot} of a few thousand degrees Kelvin [32]. Assuming the temperature of the Al_4^- cluster to be, e.g., $T_{\text{vib}} = T_{\text{rot}} = 2000$ K at the moment of injection into the trap, the average energies carried by the vibrations and rotations are 1.1 and 0.26 eV, respectively, assuming a rotational energy constant of $B_{4^-} \approx 10 \mu\text{eV}$ as estimated from the geometry of Al_4^- [24]. The corresponding average rotational angular momentum carried by the cluster is $\langle J \rangle \approx 150\hbar$. While being stored in the trap, the isolated ions cool by radiative transitions. After 100 ms of storage, the vibrational energy is known [4] to be reduced to ≈ 0.25 eV, which corresponds to a vibrational temperature of ≈ 600 K. The cooling of the rotations, however, is only moderate; each radiative transition can only change the total angular momentum by at most $1\hbar$ and after 100 ms of cooling and the emission of at most 10–20 photons, the average rotational angular momentum is expected to be still above $130\hbar$, i.e., there is still an average energy of greater than 0.20 eV stored in the rotational degrees of freedom. After laser excitation, the autodetachment of Al_4^{-*} is not expected to be influenced by the rotational energy because the moments of inertia of Al_4^- and Al_4 are very similar and the angular

momentum that can be carried away by the emitted electron is small. On the other hand, in the fragmentation process $\text{Al}_4^{-*} \rightarrow \text{Al}_3^- + \text{Al}$, the relative angular momentum of the products can be large; thus at least part of the rotational energy of Al_4^{-*} can be transferred to kinetic energy, which can lead to fragmentation for vibrational energies well below D_0 .

In the present section we use the theory of unimolecular decay based on statistical phase space and detailed balance considerations [2,3,36] to interpret our experimental data and to extract the adiabatic electron detachment and one-atom dissociation energies. Since relevant experimental knowledge of the spectroscopy of Al_4^- and Al_4 is sparse, we use theoretical predictions for the electronic and vibrational structure of these clusters. For Al_4^- we use the result of Ref. [30], which predicts, besides the electronic ground state 2A_g , an excited doublet state $^2B_{1u}$ at 0.09 eV as well as a quartet state $^4B_{3u}$ at 0.15 eV. We neglect for the time being the quartet manifold and use the six fundamental vibrational frequencies calculated for the 2A_g state to estimate the level density of Al_4^- . The electronic energies of Al_4 are taken from Ref. [30] [$^3B_{1g}$, $^3B_{1u}$ (0.11 eV), and 1A_g (0.20 eV)], while the vibrational frequencies are from Ref. [23]. For Al_3^- , we consider only the three fundamental vibrational frequencies built on the electronic 1A_1 ground state [37]. The level densities of Al_4^- , Al_4 , and Al_3^- are calculated within the harmonic-oscillator approach using the Beyer-Swinehart method [38]. To describe the rotational degrees of freedom we treat the aluminum clusters as spherical tops with average rotational energy constants of $B_{4^-} \approx 10 \mu\text{eV}$, $B_4 \approx 10 \mu\text{eV}$, and $B_{3^-} \approx 20 \mu\text{eV}$ for Al_4^- , Al_4 , and Al_3^- , respectively.

Based on the detailed balance approach, the energy dependence of the rate coefficient $k_e(E_v)$ of Al_4^{-*} for vibrational autodetachment can be approximated by

$$k_e(E_v) = c_e \int_0^{E_v - E_{\text{ad}}} \sqrt{\epsilon_e} \frac{\rho_4(E_v - E_{\text{ad}} - \epsilon_e)}{\rho_{4^-}(E_v)} d\epsilon_e, \quad (8)$$

where $\rho_{4^-}(E_v)$ and $\rho_4(E_v)$ denote the vibrational level densities of Al_4^- and Al_4 , respectively, and where we made the usual assumption that the electron-capture cross section as a function of the electron energy ϵ_e is given by the Langevin cross section [3]. The absolute scale of $k_e(E_v)$ is set by c_e , which will be determined together with the adiabatic electron attachment energy E_{ad} , as discussed below.

To determine the energy dependence of the one-atom dissociation of Al_4^{-*} into $\text{Al}_3^- + \text{Al}$ we follow the procedure outlined in Refs. [36,39], where statistical phase-space theory is used to incorporate the rotational angular momentum together with energy and angular momentum conservation into the dissociation process. Within their approach, the rate coefficient $k_f(E_v, J)$ describing the one-atom dissociation of an Al_4^{-*} ion with vibrational energy E_v and rotational angular momentum J is given by ($J \gg 1$ and is measured in units of \hbar)

$$k_f(E_v, J) = c_f \sum_{J_f=0}^{J_f^{\text{max}}} \int_{\epsilon_f^{\text{min}}(J_f)}^{\epsilon_f^{\text{max}}(J_f)} \frac{R(J; J_f, \epsilon_f)}{2J} \times \frac{\rho_{3^-}(E_v + B_{4^-} J^2 - D_0 - B_{3^-} J_f^2 - \epsilon_f)}{\rho_{4^-}(E_v)} d\epsilon_f. \quad (9)$$

Here $\rho_{4^-}(E_v)$ and $\rho_{3^-}(E_v)$ are the vibrational level densities of Al_4^- and Al_3^- , respectively, while $R(J; J_f, \epsilon_f)$ denotes the number of orbital angular momentum states available at a fixed rotational angular momentum J_f of the fragmentation product Al_3^- and a given final translational energy ϵ_f . The integration is over all ϵ_f and the sum is over all J_f consistent with energy and angular momentum conservation. The absolute scale of k_f is set by c_f , which will be determined together with the dissociation energy D_0 from the data, as discussed below.

To derive the summation and integration limits and to determine $R(J; J_f, \epsilon_f)$, we describe the radial dissociation potential by $V(r) = -C/r^4$ with $C = p e^2/2 = 50 \text{ eV } \text{Å}^4$, which results from the interaction of the charged Al_3^- ion with the neutral aluminum atom having a polarizability of $p = 6.7 \text{ Å}^3$ [40]. As angular momentum conservation requires the orbital angular momentum L of the fragments to obey $\vec{J} = \vec{J}_f + \vec{L}$ and since the kinetic energy must be positive at the centrifugal barrier, ϵ_f is constrained to

$$\epsilon_f \geq \epsilon_f^{\min}(J_f) = B_{3^-} J_f^2 + \Lambda |J - J_f|^4, \quad (10)$$

with $\Lambda = 5.3 \times 10^{-5} \text{ } \mu\text{eV}$, while the maximum of ϵ_f is given by

$$\epsilon_f^{\max}(J_f) = E_v + B_{4^-} J^2 - D_0 - B_{3^-} J_f^2. \quad (11)$$

Moreover, the maximum rotational angular momentum carried away by the Al_3^- fragment is limited by $J_f^{\max} = ([E_v + B_{4^-} J^2 - D_0]/B_{3^-})^{1/2}$. Finally, $R(J; J_f, \epsilon_f)$ is found to be

$$R(J; J_f, \epsilon_f) = 2J_f \left\{ \left[(\epsilon_f - B_{3^-} J_f^2)/\Lambda \right]^{1/4} - |J - J_f| \right\} \quad (12)$$

for $\epsilon_f^{\min} \leq \epsilon_f \leq \epsilon_f^*$

and

$$R(J; J_f, \epsilon_f) = 2J_f (J + J_f - |J - J_f|) \quad \text{for} \quad \epsilon_f^* \leq \epsilon_f \leq \epsilon_f^{\max}, \quad (13)$$

with

$$\epsilon_f^* = B_{3^-} J_f^2 + \Lambda |J + J_f|^4. \quad (14)$$

Radiative transitions in Al_4^{-*} are only expected to compete with the autodetachment rates within a very narrow window of vibrational energies with $E_v \geq E_{\text{ad}}$. We therefore approximate the radiative transition rate $k_r(E_v)$ by setting $k_r(E_v) = c_r$ and adjusting c_r to the data.

Denoting the (normalized) vibrational energy distribution of Al_4^- at the moment of the laser shot by $f_0(E_i)$ and the probability for Al_4^- to be in a rotational angular momentum state J by $g_0(J)$, the autodetachment cross section $\sigma_e(E_\lambda, t)$ and dissociation cross section $\sigma_f(E_\lambda, t)$ at time t after the absorption of a photon of energy E_λ can be calculated using

$$\sigma_\kappa(E_\lambda, t) = \sigma_{\text{abs}}^*(E_\lambda) \sum_{J=0}^{\infty} \int_{E_{\text{ad}}}^{\infty} g_0(J) f_0(E_v = E_i + E_\lambda) \times k_\kappa(E_v, J) e^{-k_{\text{tot}}(E_v, J)t} dE_v \quad (15)$$

for $\kappa = e$ and $\kappa = f$, respectively. The total decay rate constant is given by $k_{\text{tot}}(E_v, J) = k_e(E_v) + k_f(E_v, J) + k_r(E_v)$.

To apply Eq. (15), the initial probabilities need to be specified. The probability $g_0(J)$ will be assumed to be given

by a Boltzmann distribution for a rotational temperature T_{rot} , i.e.,

$$g_0(J) = N_r (2J)^2 e^{-B_{4^-} J^2 / k_B T_{\text{rot}}}, \quad (16)$$

where k_B denotes the Boltzmann constant and N_r accounts for the normalization.

The vibrational level population $f_0(E_i)$ of a cluster still being in the cooling process is usually not well described by a Boltzmann distribution for a vibrational temperature T_{vib} as it overestimates the population of higher-lying states. We therefore use an asymmetric Gaussian of the form

$$f_0(E_i) = N_v \sqrt{E_i/E_0} e^{-(E_i - E_0)^2 / 2s_0^2} \quad (17)$$

to parametrize $f_0(E_i)$, where N_v accounts for the normalization. The two parameters E_0 and s_0 are connected to a vibrational temperature T_{vib} in the following way (see also [41]): For the Boltzmann distribution at temperature T_{vib} we calculate the most probable vibrational energy E_p from the average energy $\langle E_i \rangle$ by $E_p = \langle E_i \rangle - k_B T_{\text{vib}}$. We then set $s_0 = \sqrt{k_B C_h} T_{\text{vib}}$, where C_h denotes the heat capacity of Al_4^- , and determine E_0 by $E_0 = E_p - s_0^2 / 2E_p$ such that the maximum of $f_0(E_i)$ is equal to E_p . In the temperature region relevant in the present study ($T_{\text{vib}} \lesssim 700 \text{ K}$), we find that Eq. (17) represents rather closely the Boltzmann distribution for $E_i < E_p$, while the extended tail of the Boltzmann distribution at higher excitation energies is suppressed.

Starting from Eq. (15), we can now calculate our other observables. The delayed cross sections for electron emission $\sigma_e^d(E_\lambda)$ and fragmentation $\sigma_f^d(E_\lambda)$ introduced in Sec. III C are obtained by integrating Eq. (15) over the observation time t limited by $12 \text{ } \mu\text{s} \leq t \leq 188 \text{ } \mu\text{s}$. The branching ratios $b_f(E_\lambda)$ derived in Sec. III B are given by

$$b_f(E_\lambda) = \frac{\sigma_f(E_\lambda)}{\sigma_e(E_\lambda) + \sigma_f(E_\lambda) + \sigma_1(E_\lambda) + \sigma_2(E_\lambda)}, \quad (18)$$

where $\sigma_e(E_\lambda)$ and $\sigma_f(E_\lambda)$ are obtained by integrating Eq. (15) from $t = 0$ to ∞ . Note that the two direct ionization cross sections $\sigma_1(E_\lambda)$ and $\sigma_2(E_\lambda)$ discussed in Sec. III A only contribute to the branching ratio $b_f(E_\lambda)$ for photon energies $E_\lambda > E_{\text{ad}}$. Finally, the probability $G(E_\lambda)$, introduced and roughly estimated in Sec. III A, is given by $G(E_\lambda) = [\sigma_e(E_\lambda) + \sigma_f(E_\lambda)] / \sigma_{\text{abs}}^*(E_\lambda)$.

V. RESULTS AND DISCUSSION

The statistical model as formulated in the previous section contains, besides the adiabatic electron detachment energy E_{ad} and the dissociation energy D_0 , several parameters that have to be determined from the measured data. These are the three strength parameters c_e , c_f , and c_r , as well as the two temperatures T_{vib} and T_{rot} used to characterize the internal excitation of the Al_4^- ions prior to the laser excitation. After an in-depth exploration of the parameter space, we arrived at a unique solution that reproduces our data very well as visualized by the solid red lines in Figs. 7–9. The plotted curves are for $E_{\text{ad}} = 2.18 \text{ eV}$, $D_0 = 2.34 \text{ eV}$, $T_{\text{vib}} = 540 \text{ K}$, and $T_{\text{rot}} = 1400 \text{ K}$, while the adjusted strength parameters lead to decay rate coefficients $k_\kappa(E_v, J)$ displayed in Fig. 10.

The main parameter sensitivities are the following: The high-energy slope of the delayed electron detachment cross

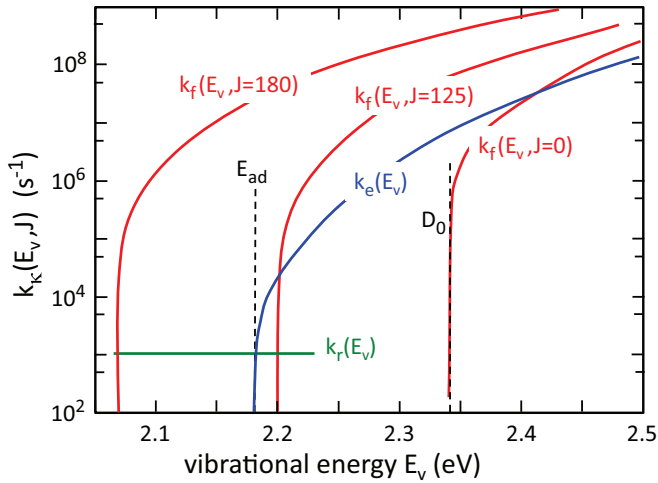


FIG. 10. (Color online) Decay rate coefficients $k_e(E_v)$, $k_f(E_v, J)$, and $k_r(E_v)$ determined from the adjustment of the statistical model to the data, assuming an adiabatic electron attachment energy of $E_{\text{ad}} = 2.18$ eV and a dissociation energy of $D_0 = 2.34$ eV for $J = 0$. The decay rate coefficients for fragmentation are given for three characteristic J values, $J = 0\hbar$, $J = \langle J \rangle = 125\hbar$, and $J = 180\hbar$, where $g_0(J)$ has dropped to half the value at the most likely J .

section $\sigma_e^d(E_\lambda)$ [see Fig. 8(b)] is shaped by the autodetachment rate coefficients $k_e(E)$; for photon energies above 2 eV an increasing number of excited Al_4^* clusters have excitation energies above $E_{\text{ad}} + 0.045$ eV such that their decay rate coefficients are greater than 10^5 s $^{-1}$ (see Fig. 10), i.e., their decays are getting too fast to be recorded within our time window for delayed events. The position of the high-energy slope determines the adiabatic electron detachment energy to $E_{\text{ad}} = (2.18 \pm 0.02)$ eV, where the uncertainty of ± 0.02 eV is mainly due to the statistics and a weak dependence of the extracted E_{ad} on the magnitude of the rate coefficient $k_e(E)$, while all other parameter dependences are negligible. For $E_\lambda \lesssim 2$ eV the shape of $\sigma_e^d(E_\lambda)$ is determined by the initial vibrational energy distribution $f_0(E_i)$ and is found to be well represented by Eq. (17) for a vibrational temperature of $T_{\text{vib}} = 540$ K as verified by the solid line in Fig. 8(b). With E_{ad} and T_{vib} being determined and the position and shape of the delayed fragmentation cross section $\sigma_f^d(E_\lambda)$ being notably independent of the dissociation energy D_0 , the shape of $\sigma_f^d(E_\lambda)$ can be used to estimate the rotational temperature. As shown by the three calculated distributions plotted in Fig. 8(a), this results in $T_{\text{rot}} = (1400 \pm 300)$ K. The one-atom dissociation energy D_0 is then determined by the total branching ratio $b_f(E_\lambda)$ for photon energies 1.80 eV $\leq E_\lambda \leq 2.18$ eV and is found to be $D_0 = (2.34 \pm 0.05)$ eV, where the uncertainty is mainly due to the statistical error of $b_f(E_\lambda)$ and the limited accuracy of T_{rot} .

The strength parameter c_f , which determines the ratio of delayed to total fragmentation, was adjusted to reproduce the absolute yield of $\sigma_f^d(E_\lambda)$. The resulting fragmentation rate coefficients $k_f(E_v, J)$ lead to a time dependence of $\sigma_f^d(E_\lambda, t)$, which is in perfect accord with the measured dependence as illustrated by the solid line in Fig. 9. The remaining two model

parameters c_e and c_r are constrained by the time dependence of $\sigma_e^d(E_\lambda, t)$ measured at $E_\lambda = 1.965$ eV and displayed in Fig. 9; the two parameters are found to be strongly correlated and the individual values are only determined to within a factor of 2. The resulting vibrational autodetachment rate coefficient $k_e(E_v)$ also influences the absolute yield of $\sigma_e^d(E_\lambda)$, however, the systematic error of the absolute scale of $\sigma_e^d(E_\lambda)$ prohibits its use in the determination of c_e . Nonetheless, as shown by the solid line in Fig. 8(b), the absolute yield of the calculated $\sigma_e^d(E_\lambda)$ agrees well with the measured one.

Finally, the branching ratios $b_f(E_\lambda)$ measured at photon energies $E_\lambda > E_{\text{ad}}$ were calculated using Eq. (18), extrapolating $\sigma_{\text{abs}}^*(E_\lambda)$ into this energy region, and using the cross-section parametrization of the two direct ionization channels introduced in Sec. III A. A reasonable overall description of $b_f(E_\lambda)$ is obtained as shown by the solid line in Fig. 7.

The two direct ionization channels have threshold energies of 2.18 ± 0.02 and 2.45 ± 0.02 eV. The lower of these two thresholds shows remarkable agreement with the adiabatic detachment energy E_{ad} determined from delayed electron emission, which supports the conjecture put forth in Sec. III A that the observed thresholds reflect the adiabatic excitation energies of the electronic states reached in Al_4 . Moreover, the two energies are consistent with the two low-energy structures seen in photoelectron spectroscopy studies of Al_4^- [12,14]. However, their association with specific transitions between the low-lying presumably strongly mixed electronic structures of Al_4^- and Al_4 needs further consideration (see also [30]).

Although the present data are nicely reproduced by our statistical model calculation and the deduced temperatures and rate coefficients are reasonable, a word of caution is needed. As discussed in Ref. [30], Al_4^- is expected to have close to the 2A_g electronic ground state an excited doublet ${}^2B_{1u}$ as well as a quartet ${}^4B_{3u}$ state. Their lifetimes are not known, but the dipole-allowed decay of the ${}^2B_{1u}$ can be expected to be in the (10–100)-ms region, while the quartet state is likely metastable in the time range relevant to the present investigation. Depending on the relative populations of these electronic states, the true $f_0(E_i)$ distribution may actually be a superposition of vibrational distributions with temperatures $\lesssim 540$ K. The vibrational level densities are calculated by using harmonic frequencies, thereby neglecting anharmonicities and centrifugal stretching effects. Moreover, treating the plane Al clusters as rigid spherical tops is certainly an oversimplification of the much richer angular momentum structure connected with deformable oblate symmetric tops. Thus, the vibrational and rotational temperatures, as well as the extracted decay rate coefficients, are likely effective temperatures and averaged rate coefficients.

Indeed, attempts to reproduce the delayed electron and fragmentation cross sections measured in Ref. [7] after 400 ms of storage by just lowering the vibrational temperature T_{vib} are not satisfying. In addition to a moderate adjustment of the decay rate coefficients and/or of the photon absorption cross section, a reduction of the rotational temperature from 1400 K to ~ 1200 K is required, while E_{ad} and D_0 stay well inside the error margins derived above. While moderate changes of the decay rate coefficients and/or of the photon absorption cross section might be attributable to a population change of the low-lying electronic states in Al_4^- , a rotational temperature

change of 200 K corresponds within the applied spherical top description to an average rotational energy change of ~ 26 meV and a ΔJ change of $\sim 10\hbar$, which is difficult to reconcile with the three or four rovibrational transitions that may take place during the additional 300 ms of radiative cooling. It remains to be seen if such a rotational energy change can be accounted for by properly describing the rotational angular momentum structure of the plane Al cluster within the oblate symmetric top model. As we are dealing with high rotational angular momenta and the centrifugal distortions of the rovibrational spectrum are expected to be sizable, we might also expect sizable violations of the K selection rules, K being the projection of J onto the symmetry axis. Since, moreover, the moment of inertia around the symmetry axis is approximately twice as large as that around the other two principle axes, a sizable amount of additional rotational energy could be carried away by rovibrational transitions with $\Delta K > 0$.

VI. CONCLUSION

The competition between electron detachment and one-atom fragmentation of laser-excited rotationally hot Al_4^{-*} clusters has been investigated. Although the adiabatic electron detachment energy E_{ad} is well below the dissociation energy D_0 , the fragmentation was found to dominate electron

detachment at all photon energies $E_\lambda < E_{ad}$. The preponderance of fragmentation is due to the rotational energy, which can be converted into translational energy between the two fragments, while this is prohibited in the electron detachment process. Our experimental findings can be well described within the unimolecular decay model based on statistical phase-space theory. The model description allowed us to determine the adiabatic detachment energy to be $E_{ad} = (2.18 \pm 0.02)$ eV and the one-atom fragmentation energy to be $D_0 = (2.34 \pm 0.05)$ eV. These values, which are in agreement with the theoretical results of [26,31], were found to be robust within their errors against finer details of the unimolecular model used. The present investigation shows that the persistent rotation of isolated molecules can have a strong influence on their fragmentation properties and special care is required to properly interpret the experimental findings.

ACKNOWLEDGMENTS

We thank Ch. Breitenfeldt for carefully reading the manuscript. This work was supported by the European sixth framework program ITS-LEIF Network and by the Israel Science Foundation (Grant No. 1242/09). D.Sc. acknowledges support from the Weizmann Institute of Science through the Joseph Meyerhoff program.

-
- [1] E. E. B. Campbell and R. D. Levine, *Ann. Rev. Phys. Chem.* **51**, 65 (2000).
- [2] J. U. Andersen, E. Bonderup, and K. Hansen, *J. Phys. B: At. Mol. Opt. Phys.* **35**, R1 (2002).
- [3] K. Hansen, *Statistical Physics of Nanoparticles in the Gas Phase*, Springer Series on Atomic, Optical, and Plasma Physics Vol. 73 (Springer, Berlin, 2013).
- [4] Y. Toker, O. Aviv, M. Erritt, M. L. Rappaport, O. Heber, D. Schwalm, and D. Zajfman, *Phys. Rev. A* **76**, 053201 (2007).
- [5] O. Aviv, Y. Toker, M. Erritt, K. G. Bhushan, H. B. Pedersen, M. L. Rappaport, O. Heber, D. Schwalm, and D. Zajfman, *Rev. Sci. Instrum.* **79**, 083110 (2008).
- [6] O. Aviv, Y. Toker, J. Rajput, D. Strasser, O. Heber, D. Schwalm, D. Zajfman, and L. H. Andersen, *Phys. Rev. A* **82**, 035201 (2010).
- [7] O. Aviv, Y. Toker, D. Strasser, M. L. Rappaport, O. Heber, D. Schwalm, and D. Zajfman, *Phys. Rev. A* **83**, 023201 (2011).
- [8] O. Aviv, B. Kafle, V. Chandrasekaran, O. Heber, M. L. Rappaport, H. Rubinstein, D. Schwalm, D. Strasser, Y. Toker, and D. Zajfman, *Rev. Sci. Instrum.* **84**, 053106 (2013).
- [9] G. Ganteför, K. H. Meiwes-Broer, and H. O. Lutz, *Phys. Rev. A* **37**, 2716 (1988).
- [10] K. J. Taylor, C. L. Petiette, M. J. Craycraft, O. Chesnovsky, and R. E. Smalley, *Chem. Phys. Lett.* **152**, 347 (1988).
- [11] W. A. Saunders, P. Fayet, and L. Wöste, *Phys. Rev. A* **39**, 4400 (1989).
- [12] C. Y. Cha, G. Ganteför, and W. Eberhardt, *J. Chem. Phys.* **100**, 995 (1994).
- [13] G. Ganteför, W. Eberhardt, H. Weidele, D. Kreisle, and E. Recknagel, *Phys. Rev. Lett.* **77**, 4524 (1996).
- [14] X. Li, H. Wu, X.-B. Wang, and L.-S. Wang, *Phys. Rev. Lett.* **81**, 1909 (1998).
- [15] J. Akola, M. Manninen, H. Hakkinen, U. Landman, X. Li, and L. S. Wang, *Phys. Rev. B* **60**, R11297 (1999).
- [16] C. M. Neal, A. K. Starace, and M. F. Jarrold, *Phys. Rev. B* **76**, 054113 (2007).
- [17] A. K. Starace, C. M. Neal, B. Cao, M. F. Jarrold, A. Aguado, and J. M. Lopez, *J. Chem. Phys.* **131**, 044307 (2009).
- [18] L. Ma, B. Issendorff, and A. Aguado, *J. Chem. Phys.* **132**, 104303 (2010).
- [19] M. W. Froese, K. Blaum, F. Fellenberger, M. Grieser, M. Lange, F. Laux, S. Menk, D. A. Orlov, R. Repnow, T. Sieber, Y. Toker, R. von Hahn, and A. Wolf, *Phys. Rev. A* **83**, 023202 (2011).
- [20] M. Lange, M. W. Froese, S. Menk, D. Bing, F. Fellenberger, M. Grieser, F. Laux, D. A. Orlov, R. Repnow, T. Sieber, Y. Toker, R. von Hahn, A. Wolf, and K. Blaum, *New J. Phys.* **14**, 065007 (2012).
- [21] J. J. Melko and A. W. Castleman, Jr., *Phys. Chem. Chem. Phys.* **15**, 3173 (2012).
- [22] T. H. Upton, *J. Chem. Phys.* **86**, 7054 (1987).
- [23] P. Calaminici, N. Russo, and M. Toscano, *Z. Phys. D* **33**, 281 (1995).
- [24] B. K. Rao and P. Jena, *J. Chem. Phys.* **111**, 1890 (1999).
- [25] J. Akola, M. Manninen, H. Hakkinen, U. Landman, X. Li, and L. S. Wang, *Phys. Rev. B* **62**, 13216 (2000).
- [26] C. G. Zhan, F. Zheng, and D. A. Dixon, *J. Am. Chem. Soc.* **124**, 14795 (2002).
- [27] J. Sun, W. C. Lu, H. Wang, Z. S. Li, and C. C. Sun, *J. Phys. Chem. A* **110**, 2729 (2006).
- [28] Y. L. Zhao and R. J. Zhang, *J. Phys. Chem. A* **111**, 7189 (2007).

- [29] R. Fournier, *J. Chem. Theory Comput.* **3**, 921 (2007).
- [30] T. Sommerfeld, *J. Chem. Phys.* **132**, 124305 (2010).
- [31] V. O. Kiohara, E. F. V. Carvalho, C. W. A. Paschoal, F. B. C. Machado, and O. Roberto-Neto, *Chem. Phys. Lett.* **568-569**, 42 (2013).
- [32] A. Wucher and B. J. Garrison, *J. Chem. Phys.* **105**, 5999 (1996).
- [33] D. Zajfman, D. Strasser, O. Heber, S. Goldberg, A. Diner, and M. L. Rappaport, *Nucl. Instrum. Methods Phys. Res. Sect. A* **532**, 196 (2004).
- [34] P. Gerhardt, M. Niemietz, Y. D. Kim, and G. Ganteför, *Chem. Phys. Lett.* **382**, 454 (2003).
- [35] M. L. Du and J. B. Delos, *Phys. Rev. A* **38**, 5609 (1988).
- [36] M. F. Jarrold, in *Cluster of Atoms and Molecules I*, edited by H. Haberland (Springer, Berlin, 1994), p. 163.
- [37] S. R. Miller, N. E. Schultz, D. G. Truhlar, and D. G. Leopold, *J. Chem. Phys.* **130**, 024304 (2009).
- [38] T. Beyer and D. F. Swinehart, *Commun. Assoc. Comput. Mach.* **16**, 379 (1973).
- [39] P. Parneix and F. Calvo, *J. Chem. Phys.* **119**, 9469 (2004).
- [40] P. Milani, I. Moullet, and W. A. de Heer, *Phys. Rev. A* **42**, 5150 (1990).
- [41] J. U. Andersen, E. Bonderup, and K. Hansen, *J. Chem. Phys.* **114**, 6518 (2001).